Deformation Time-Series Generation in Areas Characterized by Large Displacement Dynamics: The SAR Amplitude Pixel-Offset SBAS Technique

Francesco Casu, Andrea Manconi, Antonio Pepe, and Riccardo Lanari, *Senior Member, IEEE*

***Abstract*—We exploit the amplitude information of a sequence of synthetic aperture radar (SAR) images, acquired at different times, in order to generate displacement time-series in areas characterized by large and/or rapid deformation, the size of which is on the order of the image's pixel dimensions. We follow the same rationale of the Small BAseline Subset (SBAS) differential SAR interferometry (DInSAR) approach, by coupling the available SAR images into pairs characterized by a small separation between the acquisition orbits. We exploit the amplitudes of the selected image pairs in order to calculate the relative across-track (range) and along-track (azimuth) pixel-offsets (PO). Finally, we apply the SBAS inversion strategy to retrieve the range and azimuth displacement time-series. This approach, referred to as pixel-offset (PO-) SBAS technique, has been applied to a set of 25 ENVISAT SAR observations of the Sierra Negra caldera, Galápagos Islands, spanning the 2003–2007 time interval. The retrieved deformation time-series show the capability of the technique to detect and measure the large displacements affecting the inner part of the caldera that, in correspondence to the October 2005 eruption, reached several meters. Moreover, by comparing the PO-SBAS results to continuous GPS measurements, we estimate that the accuracy of the PO-SBAS time-series is on the order of 1/30th of a pixel for both range and azimuth directions.**

***Index Terms*—Differential SAR interferometry (DInSAR), Galápagos islands, SAR image pixel-offset, Small BAseline Subset (SBAS), synthetic aperture radar (SAR).**

I. Introduction

SURFACE deformation is a key information for understanding a number of natural phenomena and anthropogenic processes (seismic events, volcanic unrests, landslides, fluid exploitation, mining, etc.). Differential synthetic aperture radar (SAR) interferometry (DInSAR) [1], which exploits the phase difference between SAR image pairs acquired over the same area before and after a deformation event, allows the retrieval of spatially dense maps of ground deformation projected along the sensor line of sight (LOS) [2]–[4].

Originally applied to investigate single deformation events [5]–[9], the DInSAR technique has further been extended through the development of advanced algorithms that allow analyzing the temporal evolution of the detected displacements via the generation of deformation time-series. This result is achieved by considering a sequence of SAR images acquired at different times and properly combined in a set of differential interferograms. In this case, the deformation time-series can be computed through the inversion of the available interferograms [10]–[18] in areas where the phase signal is not significantly affected by noise (coherent areas) [19], [20]. Among several approaches, a well-established one is the Small BAseline Subset (SBAS) advanced DInSAR technique [11], which relies on an appropriate selection of the SAR image pairs involved in the generation of the exploited interferograms. These interferograms are characterized by a small spatial and temporal separation (baseline) between the acquisition orbits that reduces some of the more problematic noise sources in interferometry, particularly temporal and spatial decorrelation. The spatial baseline we consider is the component of the baseline vector perpendicular to the sensor illumination direction, often referred to as the perpendicular or orthogonal baseline. The generated set of small baseline interferograms is subsequently inverted via the singular value decomposition (SVD) technique, in order to obtain deformation time-series over coherent pixels [11]. The capability of the SBAS-DInSAR technique to accurately measure displacements in different case studies has already been well documented [21]–[27].

In areas where deformation is on the order of the SAR image pixel size, the differential interferograms begin to exhibit unfavorable characteristics that impact their usability in displacement time-series. Interferograms computed over these areas are affected by high fringe rates, leading to difficulties in the phase unwrapping step, and/or coherence losses due to significant misregistration errors [3], [4]. A pictorial representation of how the interferometric phase degrades as the displacement amount increases is given in Fig. 1.

In addition to the interferometric phase, the coherence and the SAR image amplitude information may also be used to investigate the effects of phenomena inducing surface displacements [28]. Moreover, if the deformation introduces geometric distortions without significantly affecting the SAR image reflectivity, displacements can still be retrieved by measuring

Manuscript received April 21, 2010; revised November 15, 2010; accepted December 22, 2010. Date of publication February 10, 2011; date of current version June 24, 2011. This work has been partially supported by the Italian Space Agency (ASI). The ENVISAT SAR data have been provided by the European Space Agency and WInSAR in collaboration with F. Amelung at the University of Miami. The DEM of the investigated zone was acquired through the SRTM archive.

F. Casu, A. Pepe and R. Lanari are with the Istituto per il Rilevamento Elettromagnetico dell'Ambiente, Italian National Research Council (CNR), 80124 Napoli, Italy (e-mail: casu.f@irea.cnr.it; pepe.a@irea.cnr.it; lanari.r@irea.cnr.it).

A. Manconi was with the Istituto per il Rilevamento Elettromagnetico dell'Ambiente, Italian National Research Council (CNR), 80124 Napoli, Italy. He is now with the IRPI-CNR, 10135 Torino, Italy (e-mail: andrea.manconi@irpi.cnr.it).

Digital Object Identifier 10.1109/TGRS.2010.2104325

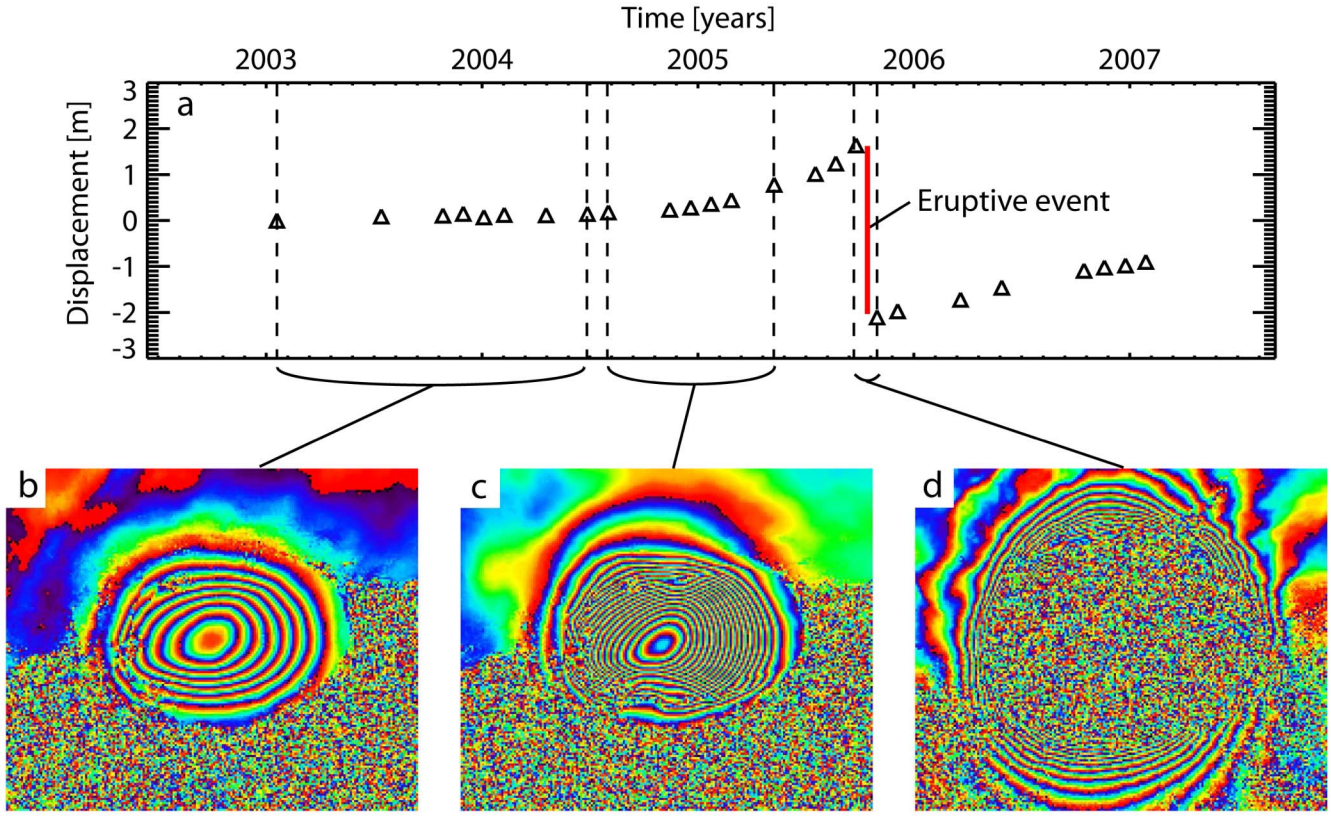

Fig. 1. Pictorial representation of the effects due to different amounts of deformation on the interferometric phase for three selected interferograms relevant to the Sierra Negra caldera (Galápagos Islands), which have been computed from the ENVISAT data analyzed in the experiments presented in Section III. (a) Plot of the deformation time-series showing the temporal evolution of the range displacements affecting the caldera center, induced by magma accumulation beneath the volcano followed by an eruptive event. (b)–(d) Differential interferograms relevant to different deformation regimes and epochs: when the deformation signal is on the order of few tens of centimeters, the interferometric phase information is fully preserved (b) and the corresponding deformation pattern can be easily retrieved; as the displacement rate increases, the corresponding fringe rate of the interferograms also increases (c), potentially leading to severe phase unwrapping errors when retrieving the corresponding deformation signal. Finally, the interferometric phase signal is completely corrupted (d) when the amount of deformation is large enough to induce misregistration errors within the investigated SAR data pair.

the distortion of the scene, as observed in the amplitudes of SAR image pairs acquired before and after the event. Indeed, amplitude-based analyses, often referred to as feature-tracking, pixel-tracking, or pixel-offset (PO) techniques, have already been successfully carried out to directly estimate the deformation field related to single deformation episodes [29]–[35].

In this work, we propose an extension of the SAR amplitude PO techniques in order to move from the investigation of single deformation events to temporally varying phenomena. Our approach follows the same rationale as the SBAS-DInSAR technique; indeed, we start by properly selecting a sequence of small baseline SAR image data pairs which have been previously co-registered with respect to a common master image [36]. Subsequently, instead of the phase difference of the selected SAR image pairs, we analyze their amplitudes in order to calculate the PO estimates for both the across-track (range) and along-track (azimuth) directions. We then apply the SVD-based inversion strategy of SBAS-DInSAR to the estimated relative range and azimuth offsets to generate the corresponding offset-based deformation time-series.

In this paper, we first describe the pixel-offset (PO-) SBAS approach. We then present results for a test case based on an ENVISAT SAR data sequence (Track: 61, Frames: 7173-7191, Swath: I2) over the Galápagos Islands. In particular, we focus our analysis on Sierra Negra caldera, an active volcanic area often characterized by large and/or rapid deformation events [37]. We investigate the performance of the PO-SBAS approach by comparing our computed deformation estimates to continuous GPS measurements acquired within the caldera. The last section of the manuscript has some concluding remarks.

II. Rationale of the Pixel-Offset SBAS Technique

Let us first briefly summarize the most relevant analytical aspects of the SBAS-DInSAR technique whose rationale is followed in the subsequently presented approach. As stated before, the SBAS technique is a DInSAR algorithm that allows detecting Earth's surface deformation and analyzing their temporal evolution by exploiting a properly selected sequence of co-registered small baseline SAR image pairs, leading to a redundant set of DInSAR interferograms. To retrieve the displacement time-series, the unwrapped phases of the interferograms are properly combined by considering the following relationship (expressed in matrix form) for each coherent pixel [11]:

$$\mathbf{B}\overline{v}_{\varphi} = \overline{\delta\varphi} \tag{1}$$

where $\overline{\delta\varphi}$ represents the estimated unwrapped phase vector (known terms), $\mathbf{B}$ is the coefficients' matrix related to

the selected interferogram data set (see [11]), and $\overline{v}_{\varphi}$ is the unknown vector representing the mean phase velocity between time adjacent SAR acquisitions. The system (1) is overdetermined and, due to the small baseline constraint, $\mathbf{B}$ might have rank deficiency if the overall data are separated into different subsets [11]. Therefore, the solution of (1) in the least square sense is obtained by applying the SVD decomposition method. This approach also provides a minimum norm constraint on the retrieved $\overline{v}_{\varphi}$ vector, guaranteeing a physically sound solution without large discontinuities in the final result [14]. Finally, to obtain the radar LOS projection of displacement time-series, an additional (but trivial) integration step of the retrieved $\overline{v}_{\varphi}$ vector is necessary, followed by an appropriate filtering of possible atmospheric artifacts [11].

Let us now move from the interferometric phase to the SAR image amplitude analysis. Accordingly, we assume to have a sequence of co-registered full resolution small baseline SAR data pairs as the ones used in the conventional SBAS-DInSAR approach, and to calculate the deformation time-series from the amplitude of the available image pairs. For this purpose, we start by computing the relative displacements for each small baseline image pair. This step is carried out by applying the normalized cross-correlation (NCC) [29], [38] technique,[1] which is widely used for SAR analyses (see [30], [31], [38], and [40]). This approach calculates a matching correlation surface (MCS) as the inner product between two oversampled SAR scenes, displaced by lags over a predefined search range in the across-track (range) and along-track (azimuth) directions [38] identified, hereafter, by the x and y variables, respectively. By carrying this step out, we compute (for each investigated pixel) an estimation of the range and azimuth shifts, finally leading to offset maps for each data pair with accuracies that are commonly on the order of 1/10th–1/20th of a pixel [30], [31]. At this stage, it is very important to provide some information on the "quality" of the retrieved offsets. In our case, since we exploit the AMPCOR Fortran routine provided in the ROI_PAC software [38], we can benefit from the computed variance values, say σ_x^2 and σ_y^2, of the two dimensional MCS maps (more analytical details on the AMPCOR routine are provided in Appendix). Note that to lower σ_x^2 and σ_y^2 values correspond to higher quality matches, and by imposing a proper threshold, it is possible to identify areas where the PO estimations are reliable for each data pair, i.e., a mask of "good" pixels. In this context, it is also important to reconsider the impact that the baseline constraints we imposed on the selected pairs may have on the retrieved PO quality. To clarify this issue, we have considered the SAR data set analyzed in the experiments provided in Section III. In particular, we computed the POs for each acquisition with respect to the same master image, thus neglecting any baseline constraint. As shown in Fig. 2(a), it is evident that the number of the reliable pixels decreases when the perpendicular baseline increases, interestingly, by following a quasi-quadratic relationship. This effect further enforces the benefit of considering the small baseline constraint in the data pairs' selection, which is implicit in the SBAS strategy, because it is also relevant for the amplitude-based SAR applications in order to maximize the number of reliable pixels. Note also that we do not consider in this case any spectral shift compensation [41] because since we focus on the amplitude information of the SAR data pairs, we do not want to degrade the spatial resolution of the exploited SAR amplitude images.

[1]We could also consider the technique based on the Fourier shift theorem [39] but we preferred the NCC algorithm family due to its consolidated exploitation in the SAR context.

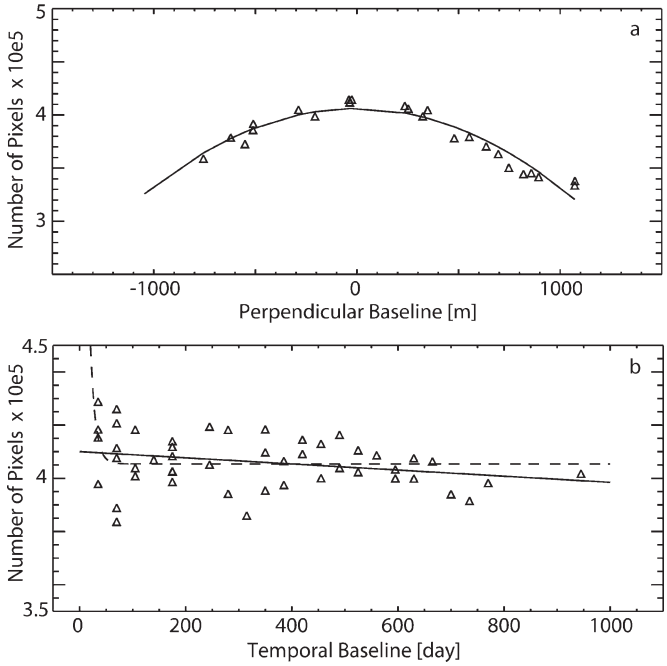

Fig. 2. Dependence of the number of reliable pixels with respect to the spatial (perpendicular) and temporal baselines for the ENVISAT data set analyzed in the experiments presented in Section III. (a) Total number of reliable pixels (triangles) with respect to the perpendicular baselines; the quadratic curve (solid line), fitting the retrieved values of the number of pixels, is also shown. (b) Total number of the reliable pixels (triangles) with respect to the temporal baselines; the best-fit linear and exponential curves, represented by the solid and dashed lines, respectively, are also shown.

Following these considerations on the spatial baseline, we also investigated the impact of the temporal one on the retrieved offsets. In particular, we computed the PO for the selected SAR data pairs analyzed in Section III by focusing on those with a perpendicular baseline not exceeding 400 m, thus mitigating the baseline-induced effects on the retrieved offset quality, see Fig. 2(a). In Fig. 2(b), we plot the computed number of reliable pixels versus the temporal baseline of exploited SAR data pairs; moreover, we also plot the best-fit linear and exponential curves [42] that are represented in Fig. 2(b) by the solid and dashed lines, respectively. Except for some data pairs with a very short time span (less than three months), the impact of the temporal baseline on the PO quality estimate is limited.

Let us now move to the analysis of the PO estimates achieved for the selected SAR data pairs. In this case, by identifying those pixels that appear reliable in a significant percentage of the investigated SAR data pairs relevant to the analyzed sequence, it is possible to select a "common mask" for the overall data set. This step is essential to identify pixels that can be investigated for the whole time period. Moreover, since the range- and azimuth-offset maps show a peculiar cross-hair artifact pattern, a spatial smoothing filtering is also applied to suppress the high-frequency noise [32].

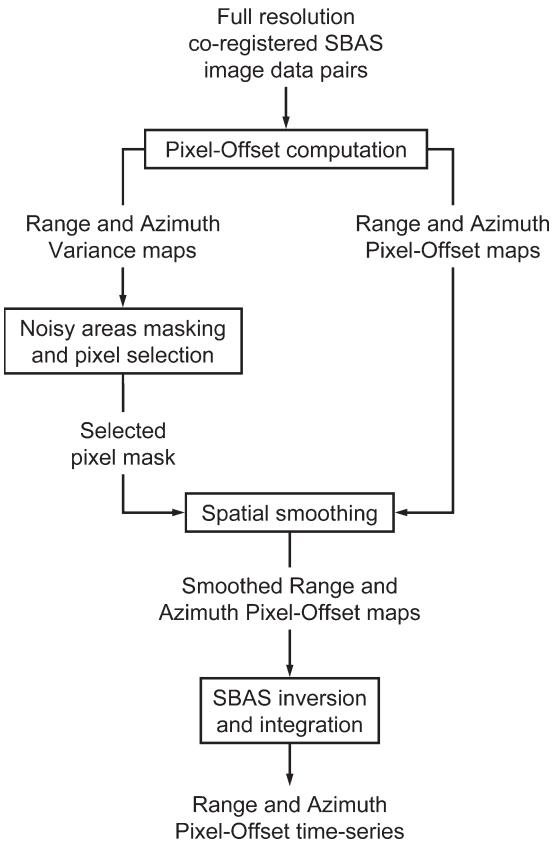

Fig. 3. Flowchart of the PO-SBAS algorithm.

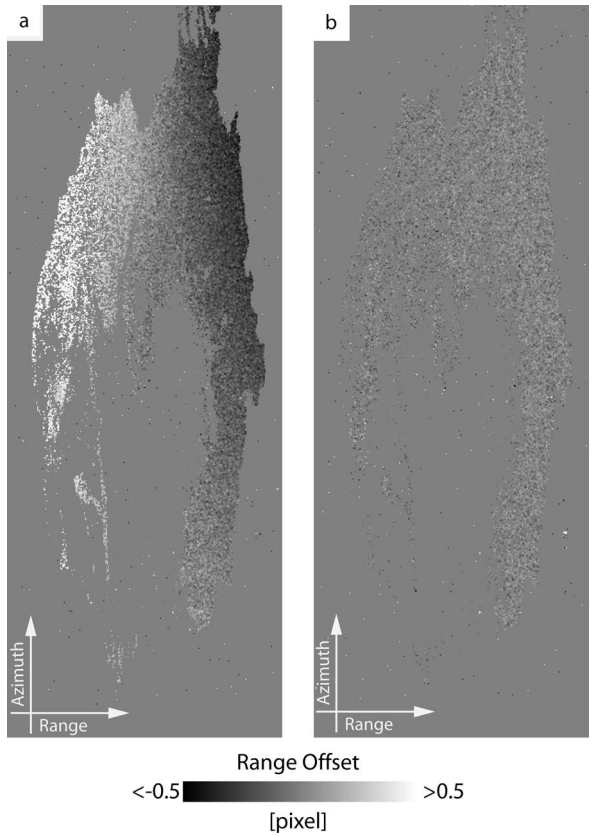

Fig. 4. Range PO estimates for the 26 April 2004–13 November 2004 ENVISAT SAR data pair, acquired over Galápagos Islands. (a) Estimated POs by co-registering for a rigid offset only. (b) Estimated POs by applying the geometric co-registration algorithm proposed in [36].

At this stage, the application of the SBAS inversion strategy to the available sequence of smoothed range and azimuth PO maps is straightforward. In particular, equivalently to (1), we consider

$$\mathbf{B}\overline{v}_x = \overline{\delta x} \tag{2}$$

$$\mathbf{B}\overline{v}_y = \overline{\delta y} \tag{3}$$

where for each investigated pixel, $\overline{\delta x}$ and $\overline{\delta y}$ represent the computed PO vectors, and $\overline{v}_x$ and $\overline{v}_y$ are the mean offset velocities between time adjacent SAR acquisitions for the range and azimuth directions, respectively. Also in this case, a final integration step is necessary to obtain the PO-SBAS time-series, for which we may generally assume the effects of possible atmospheric artifacts are negligible. The block diagram of the proposed PO-SBAS approach is sketched in Fig. 3.

It is worth noting that, for effectively applying this approach, a proper co-registration step is essential. Indeed, an incorrect co-registration may lead to uncompensated image offsets that can completely mask out the investigated displacements. Indeed, in this case, the right-hand sides of (2) and (3) become

$$\overline{\delta x} \rightarrow \overline{\delta x} + \overline{\varepsilon}_x \tag{4}$$

$$\overline{\delta y} \rightarrow \overline{\delta y} + \overline{\varepsilon}_y \tag{5}$$

where $\overline{\varepsilon}_x$ and $\overline{\varepsilon}_y$ represent the co-registration error vectors whose values may even exceed the displacement components for some data pairs.

To clarify this issue, we show in Fig. 4(a) the POs computed in the range direction for a selected SAR data pair that is not affected by significant deformation but which has been co-registered for a rigid offset only. In Fig. 4(a), it is evident the impact of the coarse co-registration step, leading to a ramp of residual POs. The importance of an appropriate fine image co-registering for surface deformation analysis is already known and the errors $\overline{\varepsilon}_x$ and $\overline{\varepsilon}_y$ in (4) and (5) can be directly estimated from the SAR data pairs and subsequently corrected. However, in order to simplify the processing and to reduce the computational load, we follow a different approach based on the geometric co-registration algorithm proposed in [36], which exploits precise orbit information and an external DEM of the investigated area to directly compute the $\overline{\varepsilon}_x$ and $\overline{\varepsilon}_y$ factors. Accordingly, a co-registration step can be directly achieved by using this information with no need for any further estimation. The effectiveness of this kind of approach is evident by considering the estimated residual POs for the same image pair of Fig. 4(a) but after such a geometric co-registration step; see Fig. 4(b). Accordingly, this technique is applied to process all the SAR data pairs exploited in this paper.

In the following, we present the results achieved by applying the described PO-SBAS approach to a data set of 25 fine co-registered ENVISAT SAR images relevant to the Galápagos Islands, spanning the 2003–2007 time interval.

TABLE I
LIST OF THE AVAILABLE ENVISAT SAR ACQUISITIONS (TRACK: 61, FRAMES: 7173-7191, SWATH: I2). NOTE THAT THE SYMBOL $B_\perp$ REPRESENTS THE PERPENDICULAR BASELINE

Day	Month	Year	$B_\perp$ [m]	Orbit
18	01	2003	552.56	04624
12	07	2003	857.87	07129
25	10	2003	-35.77	08632
29	11	2003	-39.74	09133
03	01	2004	-511.82	09634
07	02	2004	-206.78	10135
17	04	2004	-551.45	11137
26	06	2004	695.21	12139
31	07	2004	-25.70	12640
13	11	2004	1072.40	14143
18	12	2004	819.21	14644
22	01	2005	0.00	15145
26	02	2005	636.00	15646
07	05	2005	-755.61	16648
16	07	2005	-621.20	17650
20	08	2005	347.40	18151
24	09	2005	-287.98	18652
29	10	2005	-510.39	19153
03	12	2005	893.91	19654
18	03	2006	478.80	21157
27	05	2006	747.13	22159
14	10	2006	235.09	24163
18	11	2006	1071.64	24664
23	12	2006	252.57	25165
27	01	2007	323.83	25666

III. SIERRA NEGRA CALDERA: SAR DATA AND TEST SITE DESCRIPTION

Sierra Negra caldera is the most active among the shield volcanoes located in Isabela Island, Galápagos Archipelago. Sierra Negra caldera erupted in October 2005, interrupting a period of quiescence that lasted almost 30 years [43]. The investigation of geodetic signals, including GPS and DInSAR analyses, revealed at Sierra Negra an almost-continuous uplift phase, which apparently started in 1992, accelerated in the 2002–2005 period, and finally reached some meters of cumulative ground displacement before the eruption [44]. On the other hand, the October 2005 eruptive event induced an impressive subsidence event of the inner caldera [32].

Due to the large deformation dynamics affecting Sierra Negra, the retrieval of ground displacements within the inner caldera by using DInSAR techniques is a challenging task. To clarify this issue, we applied the standard SBAS-DInSAR approach to a data set of 25 ENVISAT SAR acquisitions relevant to the Galápagos Islands and spanning the 2003–2007 time interval (see Table I) in order to retrieve the corresponding deformation time-series. Note that in this study, we selected 74 data pairs (Fig. 5) with a maximum perpendicular and temporal baselines of 400 m and 1500 days, respectively. Fig. 6(a) shows the overall mean deformation velocity map retrieved via the SBAS-DInSAR analysis relevant to the investigated period and demonstrate that the DInSAR technique provides only a partial "picture" of the deformation at Sierra Negra caldera, see Fig. 6(b). Indeed, the behavior of the northern flanks of the volcano is clearly imaged, being the displacements on the order of several centimeters, and is in agreement with previous studies; see [44] and Fig. 6(c). On the contrary, displacements around the crater and inner caldera cannot be reliably retrieved, due to the lack of coherence caused by the large displacement dynamics that are in the order of the pixel dimensions (about 4 and 8 m in azimuth and range direction, respectively); see Fig. 1(d). Therefore, in order to image the spatial and temporal evolution of the deformation also in these areas, we exploit the SAR amplitude information by applying the previously described PO-SBAS approach.

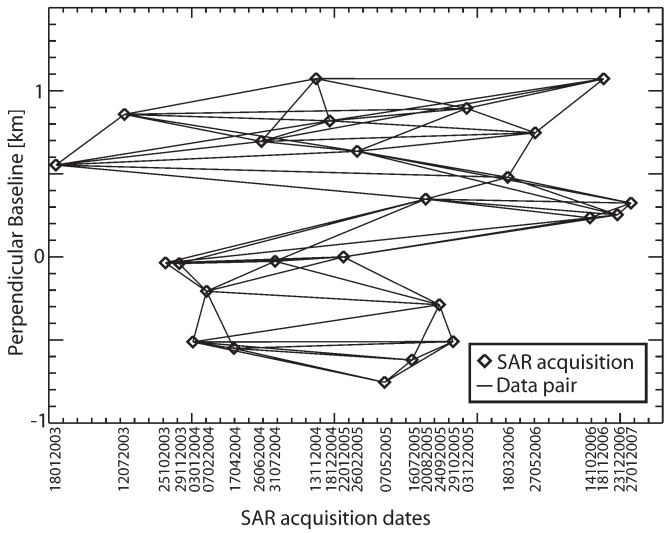

Fig. 5. Selected SBAS data pairs generated from the ENVISAT data archive shown in Table I relevant to the Galápagos Islands. Date format is "ddmmyyyy".

IV. PO-SBAS ANALYSIS: ALGORITHM IMPLEMENTATION, RESULTS, AND VALIDATION

The starting point of the PO-SBAS analysis is the calculation, via the exploited AMPCOR routine (see Appendix), of the POs and the corresponding variance values σ_x^2 and σ_y^2 for all the selected small baseline SAR image pairs, which are the same considered for the generation of the SBAS-DInSAR time-series (Fig. 5). Subsequently, we select a common mask of "good" pixels by considering those with values of σ_x^2 and σ_y^2 lower than 0.005 and present in a large percentage (we assume not less than 70%) of the all data set. Finally, we apply a spatial smoothing of 7 pixels in range and 15 in azimuth, to take into account the different spatial resolutions, and for mitigating possible noise effects [32]. At this stage, we generate the pixel time-series by inverting the offsets, computed for each data pairs, via the SBAS approach; see Fig. 3. Note that the analyzed pixel grid is selected with a step of 16 samples on both azimuth and range directions, because this is appropriate for investigating phenomena at the spatial scale of 100 m, consistently with what is already done through the SBAS-DInSAR approach.

In order to perform the PO-SBAS analysis, two key parameters must be selected; they are represented by the size of the matching window surrounding each investigated pixel, and the oversampling factor of the matching correlation surface

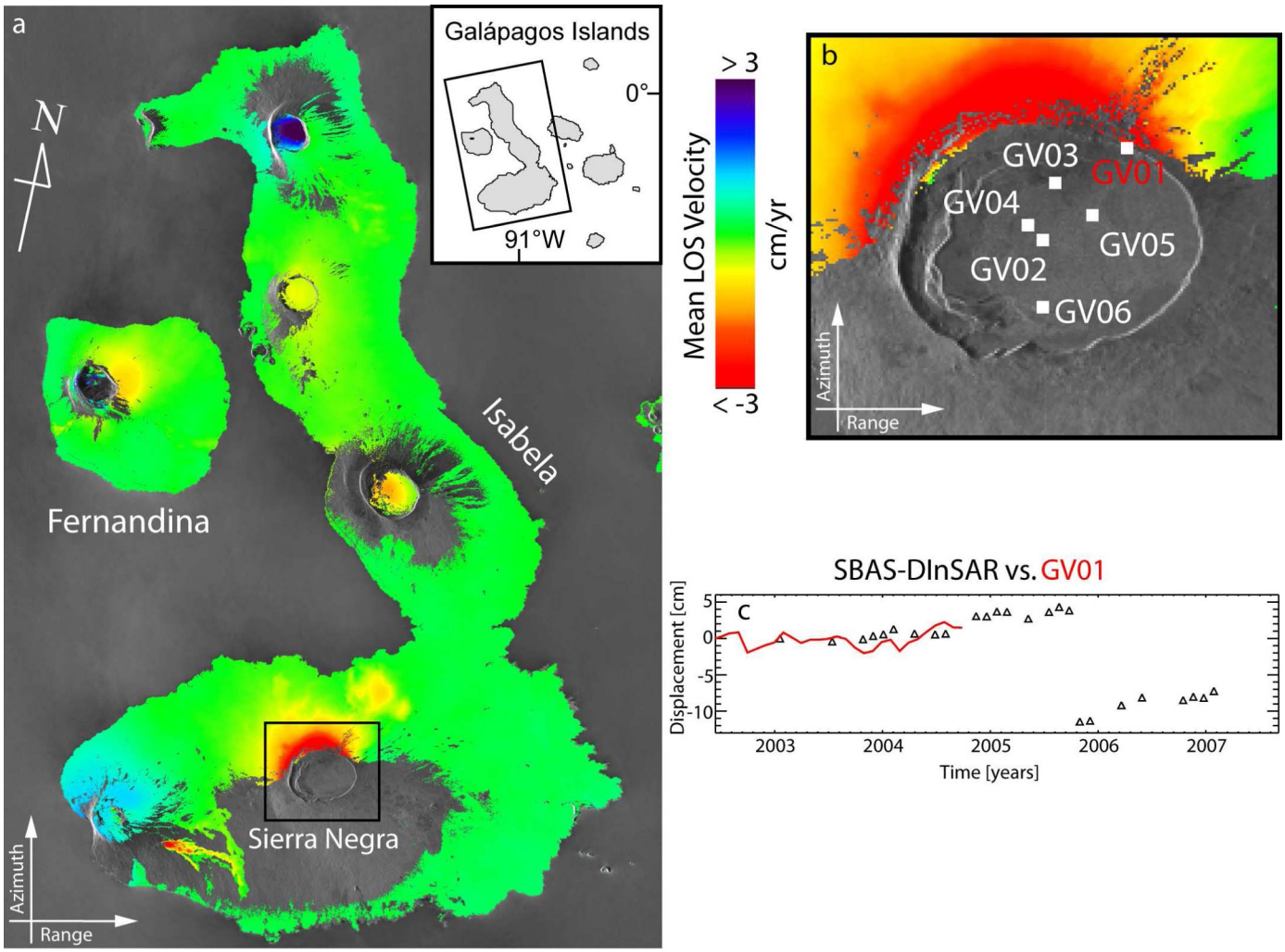

Fig. 6. SBAS-DInSAR results. (a) Mean deformation velocity map (in SAR coordinates) of the Galápagos Islands (see the inset) retrieved via the SBAS-DInSAR technique applied to the ENVISAT interferograms computed from the data pairs shown in Fig. 5. (b) Zoom of the study area, identified by the black square in (a), relevant to the Sierra Negra caldera. Note that no SBAS-DInSAR measurements are present in the inner part of the caldera due to the large deformations (on the order of several meters) caused by the October 2005 eruption. The white squares represent the station locations of the continuous GPS network deployed since 2002. (c) Comparison between the SBAS-DInSAR time-series (black triangles) and the LOS projected GPS measurements (red line) in correspondence to the GPS station labeled as GV01 [its location is shown in (b)].

retrieved by our estimation. In the following, we want to investigate the impact on the final estimates of the POs of different selections for these two parameters.

To this end, we concentrate on the Sierra Negra caldera area and we apply the PO-SBAS approach to our SAR data pairs by varying the oversampling factor and the matching window size. While the impact of the former factor does not seem particularly relevant, this is not the case for the latter one; to clearly show this effect, we present in Fig. 7 the impact of the different matching window sizes on the PO-SBAS retrieved masks of "good" pixels. Based on Fig. 7, it is clearly visible that when using a matching window size of at least 32×32 pixels, the PO-SBAS analysis is able to estimate deformation in the inner part of the caldera where the SBAS-DInSAR approach completely fails; see Fig. 6(b). Moreover, in the inner caldera area, we note a clear increment of the mask pixel number while increasing the matching window sizes. Despite this evident impact on the investigated area coverage, we remark that at this stage, no information are available with respect to the accuracy of the retrieved PO-SBAS time-series, depending on the oversampling factor and matching window size. Accordingly, in order to solve this issue, we compare our PO-SBAS results to the independent measurements of the deformation field at Sierra Negra caldera, provided by the continuous GPS stations running at Sierra Negra caldera since 2002; see Fig. 6(b). We perform our validation analysis by comparing the PO-SBAS measurements to the GPS displacement time-series reported in [44], spanning the 2003–2005 time period only. Since the PO-SBAS technique retrieves across- and along-track offsets, we have to project the three GPS displacement components (East, North, and Vertical) to make them comparable to the SAR-based estimations. However, the available GPS time-series are relevant to the North and Vertical components, while for the East one, only its average value is provided over the observed period [44]. In any case, since the ENVISAT flight track is only about 10° off from North, the PO-SBAS azimuth estimations can be effectively compared to the North GPS displacement component. More critical is the analysis of the

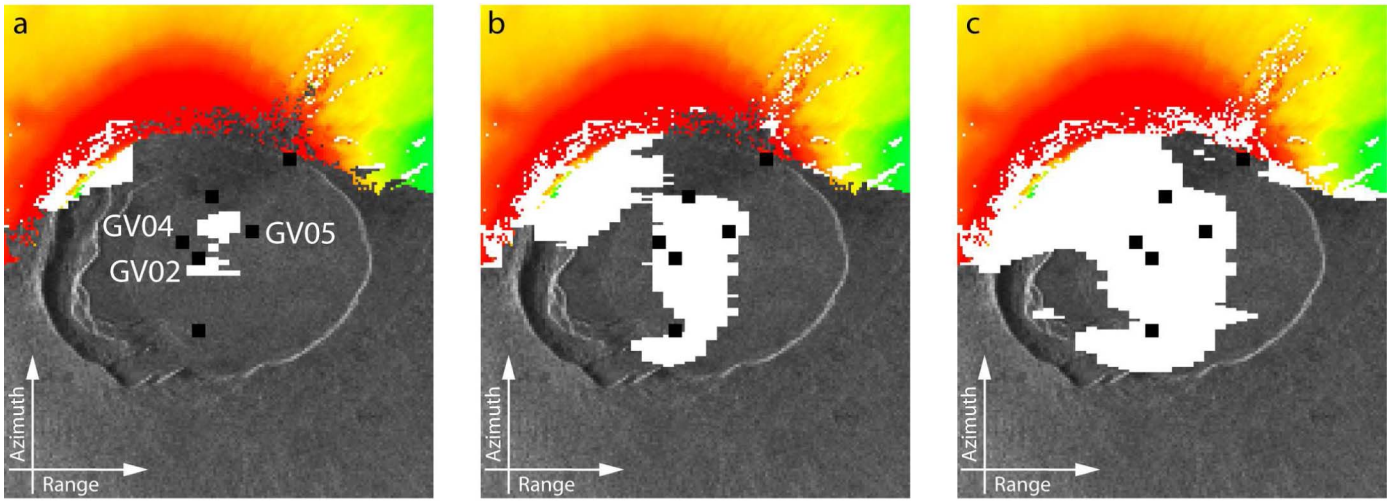

Fig. 7. Impact of the different matching window sizes on the PO-SBAS retrieved masks of "good" pixels (in white). Selected matching window sizes are of (a) 32 × 32, (b) 64 × 64 and (c) 128 × 128 pixels, respectively. Note that the GPS station locations (black squares) as well as the SBAS-DInSAR mean deformation velocity (in colors) are also shown.

TABLE II
STANDARD DEVIATIONS (IN METERS) OF THE DIFFERENCE BETWEEN THE PO-SBAS AND THE GPS TIME-SERIES IN CORRESPONDENCE TO THE GPS STATIONS LABELED AS GV02, GV04, AND GV05 IN FIG. 7(a)

Matching window size		Over	GV02 Rg	GV02 Az	GV04 Rg	GV04 Az	GV05 Rg	GV05 Az
	32†	16	0.297	0.078	0.239	0.078	0.257	0.100
		32	0.294	0.079	0.238	0.078	0.257	0.100
		64	0.295	0.079	0.238	0.078	0.257	0.100
	64	16	0.239	0.096	0.230	0.114	0.257	0.117
		32	0.238	0.099	0.231	0.117	0.262	0.119
		64	0.239	0.098	0.231	0.116	0.261	0.118
	128	16	0.241	0.113	0.265	0.127	0.275	0.144
		32	0.241	0.115	0.266	0.128	0.274	0.145
		64	0.242	0.114	0.266	0.128	0.274	0.144

Note that for the 32x32 matching window size we had to select the pixels nearest to the considered GPS station.

PO-SBAS range measurements because they are sensitive to both the Vertical and the East deformation components. However, we found that for three GPS stations, labeled as GV02, GV04, and GV05 in Fig. 7(a), the available average East motions, projected along the satellite's LOS, contributes for less than 10% of the total displacements. Therefore, we may reliably assume for these stations that the GPS East component can be considered negligible, compared to the Vertical one, and we can effectively compare the LOS projected GPS vertical displacements to the PO-SBAS range time-series.

To provide a quantitative estimation of the obtained accuracies, we calculated the standard deviation of the difference between the PO-SBAS and the GPS time-series, which are summarized in Table II. Based on these results, a dependence of the measurement accuracy from the matching window size is noticed. Moreover, as already said, the oversampling factor shows no significant impact on the PO-SBAS estimate accuracies for values greater than 16. In any case, from Table II, the estimated POs always show standard deviation values lower than 0.3 and 0.15 m for the range and azimuth directions, respectively, which correspond to accuracies on the order of 1/30th of a pixel.

In the following, we consider the PO-SBAS time-series obtained by imposing a 64 × 64 matching window size and an oversampling factor of 64 that represents a good compromise between spatial coverage, PO accuracy, and computing time. Accordingly, we present in Fig. 8(a)–(f) the comparison between the selected GPS time-series and the PO-SBAS measurements obtained with the chosen matching window size and oversampling factor; in this case, we also show the deformation patterns retrieved in correspondence to the October 2005 eruption; see Fig. 8(g) and (h).

It is evident from Fig. 8 that the PO-SBAS results complete quite nicely those obtained via the classical SBAS-DInSAR. Moreover, in the common areas, we have computed the standard deviation of the difference between the SBAS-DInSAR and the PO-SBAS deformation time-series. The histogram of the standard deviation, plotted in Fig. 9, shows a mean value of about 12 cm. By assuming a standard deviation of about 1 cm for the SBAS-DInSAR measurements [23], this further confirms that a range PO accuracy on the order of 1/30th of a pixel represents an appropriate estimate.

V. DISCUSSION AND CONCLUSION

We present in this paper a new approach to investigate the temporal evolution of large and/or rapidly varying surface deformation phenomena, from a sequence of SAR images acquired at different times. In particular, we analyze the amplitude of the available images that are coupled into small baseline pairs, similar to the SBAS-DInSAR approach. From the amplitude of the selected pairs, we estimate the relative range and azimuth amplitude POs through the NCC algorithm implementation provided by the AMPCOR Fortran routine of the ROI_PAC software. Subsequently, by following the same strategy as the SBAS-DInSAR technique, we retrieve the deformation time-series via a SVD-based inversion of the PO measurements computed for both range and azimuth directions.

We first remark that, at least in principle, the POs computed through cross-correlation analysis carried out on the amplitude

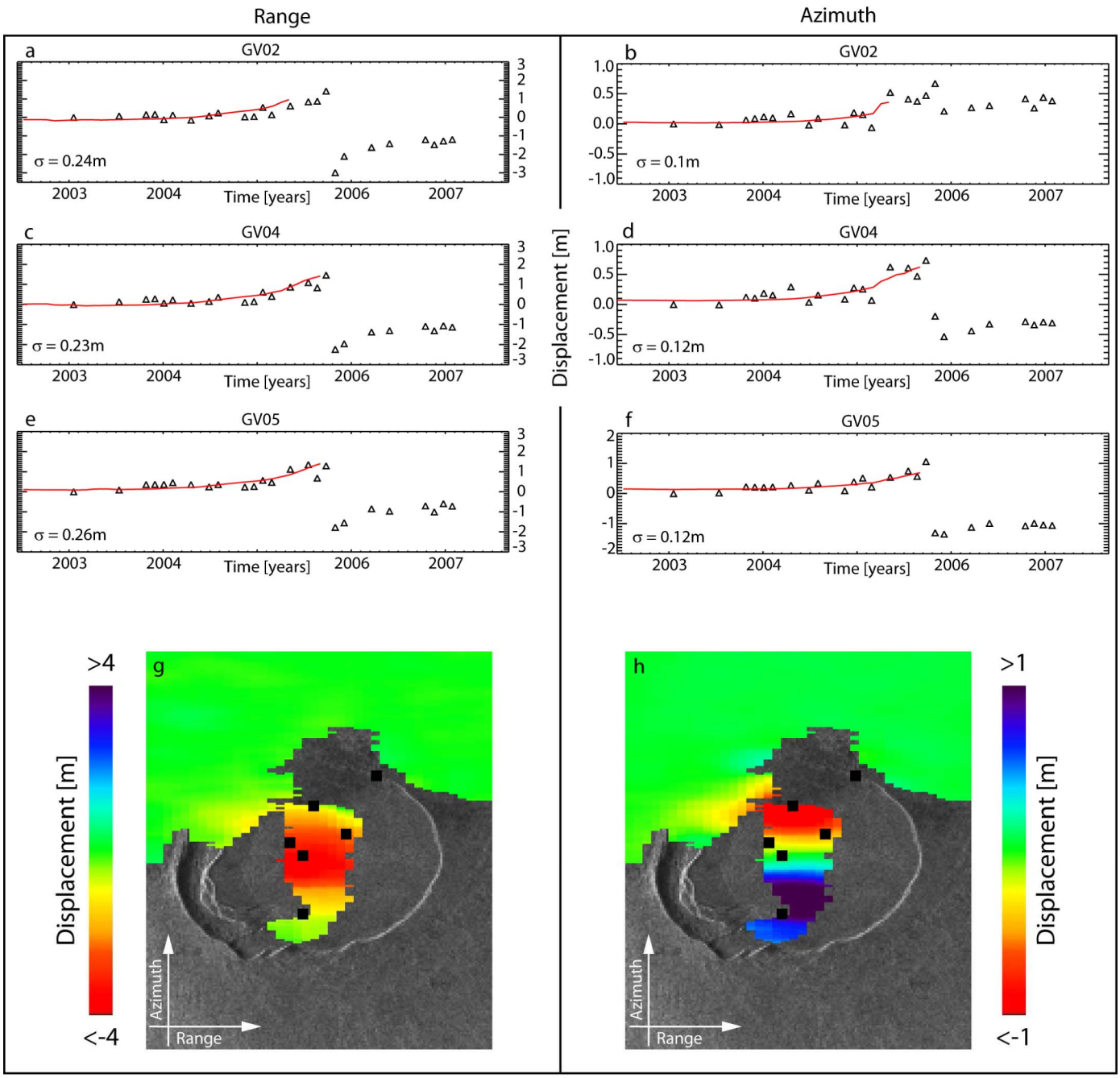

Fig. 8. PO-SBAS time-series obtained by imposing a 64 × 64 matching window size and an oversampling factor of 64. (a)–(f) comparison between the GPS time-series (red line) and the PO-SBAS measurements (black triangles) along the range and azimuth directions, in correspondence to the three GPS station labeled as GV02, GV04, and GV05 [see Fig. 7(a)]. The standard deviations of the difference between the two measurements are also reported. (g) PO-SBAS range deformation patterns retrieved in correspondence to the October 2005 eruption. (h) Same as (g) but for the azimuth direction.

component of the SAR image pairs could be replaced by alternative solutions, such as the multiple aperture interferometry system [45]. In other words, the PO-SBAS approach needs robust offset estimates at the scale of the pixel (or significant fraction of it), but it is not necessarily "locked" to the exploitation of the amplitude image information.

The PO-SBAS technique we present has been applied to an ENVISAT data set relevant to the Sierra Negra caldera, Galápagos Islands. The retrieved deformation time-series show the capability of this technique to detect and measure the large displacements affecting the inner part of the caldera that, in correspondence to the October 2005 eruption, reached several meters. Moreover, through comparison with independent information available through GPS data, the PO-SBAS measurements have been validated, leading to an estimated accuracy on the order of 1/30th of a pixel in both range and azimuth directions. Although these values are larger with respect to those achievable through conventional SBAS-DInSAR analyses, the PO-SBAS technique allows us to measure the displacements in areas where deformation is on the order of the pixel dimension, which is extremely critical for DInSAR analyses (see Fig. 1). Accordingly, the PO-SBAS approach can be very effective for

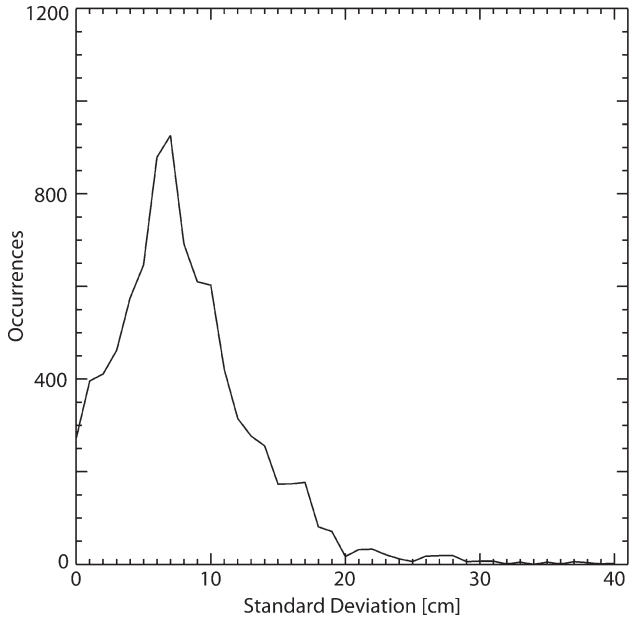

Fig. 9. Histogram of the standard deviation of the difference between the SBAS-DInSAR and the PO-SBAS range deformation time-series computed in the areas common to the two measurements.

the investigation of deformation phenomena affecting volcanic and seismogenic areas. Indeed, this approach allows retrieving spatially dense measurements in the near field of the deformation pattern, as shown for the Sierra Negra caldera test case. Another advantage of the PO-SBAS technique is its capability to easily generate along-track displacement time-series (mostly North–South), which are typically not retrieved with the currently available space-based DInSAR techniques.

The proposed approach can be trivially integrated with the conventional SBAS-DInSAR procedure to fully exploit both the phase and amplitude information available through the complex SAR data, in order to deeply investigate the temporal evolution and the spatial extent of the deformation process. Moreover, the PO-SBAS estimates can be further exploited to properly coregister the SAR data pairs, thus "restoring" the possibility of generating interferogram sequences by following the rationale proposed by [32] for a single interferogram.

We do not expect that our approach should critically depend on the deformation pattern peculiarities, if the investigated phenomena preserve the SAR amplitude image characteristics and are sufficiently spatially extended. On the other hand, we are aware that the presented results are focused on a single case study. Hence, it is certainly worthwhile for future analyses the investigation of other test areas characterized by large deformation dynamics, in order to assess for which kind of phenomena the proposed technique is appropriate. In this context, however, it is worth remarking that the deformation retrieval capability of the PO measurements obviously improves when the azimuth and range spatial resolution increases, which is the case of the new high-resolution SAR systems, such as ALOS PALSAR, TerraSAR-X, and COSMO-SkyMed. Therefore, the application of techniques like the proposed PO-SBAS approach may open new scenarios in the analysis of the Earth's surface displacements.

APPENDIX

We provide in this section some analytical details of the algorithm implemented by the AMPCOR routine, which is available in the ROI_PAC software distribution [38].

Let us start by considering two SAR images, we refer to as Reference (R) and Search (S) respectively, that we assumed are already co-registered (at least) for a rigid offset. On R, we identify a grid of pixels for which the POs will be estimated. Note that, at least in principle, it is possible to calculate the PO for every image pixel, although for many applications it is enough to consider a sparser grid, thus reducing the computing time.

Subsequently, the matching windows surrounding each identified pixel are extracted from the two images to be exploited in the PO computation, being X and Y the window dimensions along the range and azimuth directions, respectively.

Once all the matching windows have been identified in the R and S images, the normalized cross-correlation between their amplitudes is computed. In particular, the inner product of the R image with the S image is calculated, the latter being iteratively shifted along range and azimuth; the applied shifts (offsets), say i and j, respectively, belong to the intervals $-N/2 \leq i \leq N/2$ and $-M/2 \leq j \leq M/2$. Note that for each applied offset a correlation value is computed, thus permitting calculation of the corresponding matching correlation surface (MCS), whose ith and jth element for the generic pixel of range and azimuth coordinates (x, y) is the following:

$$MCS(i,j) = \frac{\sigma_{RS_{i,j}}}{\sigma_R \sigma_{S_{i,j}}} \tag{A1}$$

where

$$\sigma_R = \sqrt{\frac{\sum_{x=1,y=1}^{X,Y} |R(x,y)|^2}{XY} - \mu_R^2}$$

$$\sigma_{S_{i,j}} = \sqrt{\frac{\sum_{x=1,y=1}^{X,Y} |S(x+i,y+j)|^2}{XY} - \mu_{S_{i,j}}^2} \tag{A2}$$

are the standard deviation values for the R and S amplitude images, respectively, computed on the matching window pixels. Moreover

$$\mu_R = \frac{\sum_{x=1,y=1}^{X,Y} |R(x,y)|}{XY}$$

$$\mu_{S_{i,j}} = \frac{\sum_{x=1,y=1}^{X,Y} |S(x+i,y+j)|}{XY} \tag{A3}$$

are the corresponding mean values and

$$\sigma_{RS_{i,j}} = \frac{\sum_{x=1,y=1}^{X,Y} |R(x,y)|\,|S(x+i,y+j)|}{XY} - \mu_R \mu_{S_{i,j}} \tag{A4}$$

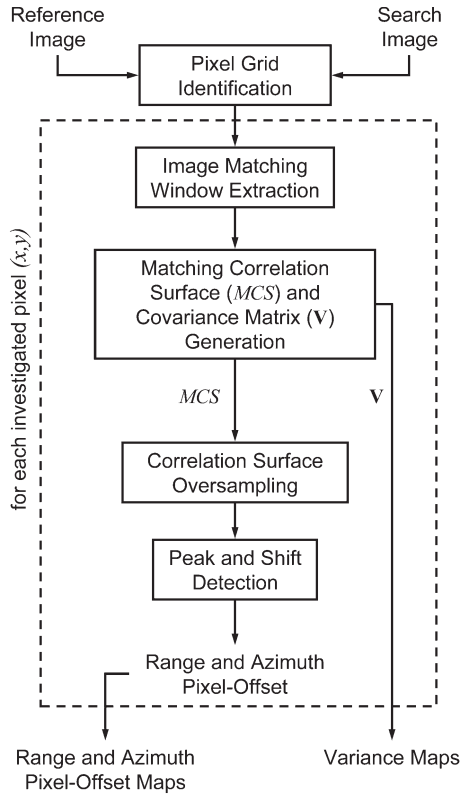

Fig. 10. AMPCOR routine flowchart.

the covariance term. Note that the analyzed images are always oversampled by a factor of two, allowing offset estimates to half a pixel. Moreover, the matching algorithm is time-domain-based, in order to analyze data also presenting some "holes" (i.e., missing pixels).

After computing the MCS, its peak position is identified, providing a first estimate of the required PO; the obtained MCS is then oversampled (typically by a factor of 32 or 64) and interpolated via a $sinc$ function around its peak. Accordingly, it is possible to search for the position of the correlation peak on a subpixel basis, giving us the final PO estimates.

In addition to the offset measurements, an estimate of their accuracy is also assessed; it depends on the noise level

$$n = 1 - \max(MCS) \tag{A5}$$

and on the curvature of the correlation surface around its peak, with sharper peak shapes indicating more reliable offset estimates. More formally, the accuracy of the offset measurements is assessed by considering the covariance matrix, say $\mathbf{V}$, which in our case is a function of the local noise level and of the MCS Hessian matrix.

The covariance matrix is expressed as follows:

$$\mathbf{V} = \begin{pmatrix} \sigma_x^2 & \sigma_{xy} \\ \sigma_{yx} & \sigma_y^2 \end{pmatrix} \tag{A6}$$

where the main diagonal values represent the offset measurement variances, providing an estimate of the retrieved offset accuracy. Because no compact form for the expressions of the $\mathbf{V}$ elements are available they have been omitted for brevity.

Note also that in addition to V, the algorithm also provides an estimate of the signal-to-noise ratio (SNR). It is represented by the ratio of the correlation surface's peak to the mean of the surrounding values, i.e.,

$$SNR = \frac{\max(MCS^2)}{\frac{\left[\sum_{i=1,j=1}^{N,M} MCS^2(i,j)\right] - \max(MCS^2)}{NM}}. \tag{A7}$$

Although the SNR is an indicator of matching accuracy, it usually is not a robust metric and it is impossible to identify absolute thresholds that work well, even for the same type of imagery. Accordingly, this information is typically used only to remove bad matches but it cannot be exploited to assess the estimated offset accuracy.

The above discussed procedure, illustrated in the flowchart of Fig. 10, is repeated for each pixel of the selected grid, permitting us to retrieve a map of the residual POs with the corresponding variances.

ACKNOWLEDGMENT

The authors would like to thank M. Manzo for the SBAS-DInSAR results generation. Moreover, the authors benefited of the discussions on the use of the AMPCOR routine of the ROI_PAC tool (ROI_PAC is an open source InSAR software developed by JPL and CalTech) with P. Lundgren, P. Rosen, E. Fielding, M. Pritchard, and particularly, with S. Hensley, whose help was essential for completing the Appendix section. We are also indebted with P. Lundgren for his proof reading of the revised manuscript and with two anonymous reviewers for their valuable remarks and suggestions.

REFERENCES

[1] A. K. Gabriel, R. M. Goldstein, and H. A. Zebker, "Mapping small elevation changes over large areas: Differential interferometry," *J. Geophys. Res.*, vol. 94, no. B7, pp. 9183–9191, 1989.

[2] P. A. Rosen, S. Hensley, I. R. Joughin, F. K. Li, S. N. Madsen, E. Rodriguez, and R. M. Goldstein, "Synthetic aperture radar interferometry," *Proc. IEEE*, vol. 88, no. 3, pp. 333–382, Mar. 2000, DOI: 10.1109/5.838084.

[3] R. Bamler and P. Hartl, "Synthetic aperture radar interferometry," *Inverse Probl.*, vol. 14, no. 4, pp. R1–R54, Aug. 1998.

[4] G. Franceschetti and R. Lanari, *Synthetic Aperture Radar Processing*. Boca Raton, FL: CRC Press, 1999.

[5] D. Massonnet, M. Rossi, C. Carmona, F. Ardagna, G. Peltzer, K. Feigl, and T. Rabaute, "The displacement field of the Landers earthquake mapped by radar interferometry," *Nature*, vol. 364, no. 6433, pp. 138–142, Jul. 1993.

[6] G. Peltzer and P. A. Rosen, "Surface displacement of the 17 May 1993 Eureka Valley, California earthquake observed by SAR interferometry," *Science*, vol. 268, no. 5215, pp. 1333–1336, Jun. 1995.

[7] D. Massonnet, P. Briole, and A. Arnaud, "Deflation of Mount Etna monitored by spaceborne radar interferometry," *Nature*, vol. 375, no. 6532, pp. 567–570, Jun. 1995.

[8] R. M. Goldstein, H. Engelhardt, B. Kamb, and R. M. Frolich, "Satellite radar interferometry for monitoring ice-sheet motion—Application to an Antarctic ice stream," *Science*, vol. 262, no. 5139, pp. 1525–1530, Dec. 1993.

[9] F. Amelung, D. L. Galloway, J. W. Bell, H. A. Zebker, and R. J. Laczniak, "Sensing the ups and downs of Las Vegas: InSAR reveals structural control of land subsidence and aquifer-system deformation," *Geology*, vol. 27, no. 6, pp. 483–486, Jun. 1999.

[10] A. Ferretti, C. Prati, and F. Rocca, "Permanent scatterers in SAR interferometry," *IEEE Trans. Geosci. Remote Sens.*, vol. 39, no. 1, pp. 8–20, Jan. 2001.
[11] P. Berardino, G. Fornaro, R. Lanari, and E. Sansosti, "A new algorithm for surface deformation monitoring based on small baseline differential SAR interferograms," *IEEE Trans. Geosci. Remote Sens.*, vol. 40, no. 11, pp. 2375–2383, Nov. 2002.
[12] C. Werner, U. Wegmüller, T. Strozzi, and A. Wiesmann, "Interferometric point target analysis for deformation mapping," in *Proc. IGARSS*, Jul. 21–25, 2003, vol. 7, pp. 4362–4364.
[13] O. Mora, J. J. Mallorquí, and A. Broquetas, "Linear and nonlinear terrain deformation maps from a reduced set of interferometric SAR images," *IEEE Trans. Geosci. Remote Sens.*, vol. 41, no. 10, pp. 2243–2253, Oct. 2003.
[14] R. Lanari, O. Mora, M. Manunta, J. J. Mallorquì, P. Berardino, and E. Sansosti, "A small baseline approach for investigating deformation on full resolution differential SAR interferograms," *IEEE Trans. Geosci. Remote Sens.*, vol. 42, no. 7, pp. 1377–1386, Jul. 2004.
[15] A. Hooper, H. Zebker, P. Segall, and B. Kampes, "A new method for measuring deformation on volcanoes and other natural terrains using InSAR persistent scatterers," *Geophys. Res. Lett.*, vol. 31, no. 23, p. L23 611, Dec. 2004, DOI: 10.1029/2004GL021737.
[16] M. Crosetto, B. Crippa, and E. Biescas, "Early detection and in-depth analysis of deformation phenomena by radar interferometry," *Eng. Geol.*, vol. 79, no. 1/2, pp. 81–91, Jun. 2005.
[17] A. Hooper, "A multi-temporal InSAR method incorporating both persistent scatterer and small baseline approaches," *Geophys. Res. Lett.*, vol. 35, no. 16, p. L16 302, 2008. DOI: 10.1029/2008GL034654.
[18] P. Shanker and H. Zebker, "Persistent scatterer selection using maximum likelihood estimation," *Geophys. Res. Lett.*, vol. 34, no. 22, p. L22 301, 2007, DOI: 10.1029/2007GL030806.
[19] H. A. Zebker and J. Villasenor, "Decorrelation in interferometric radar echoes," *IEEE Trans. Geosci. Remote Sens.*, vol. 30, no. 5, pp. 950–959, Sep. 1992.
[20] M. Coltelli, G. Fornaro, G. Franceschetti, R. Lanari, M. Migliaccio, J. R. Moreira, K. P. Papathanassiou, G. Puglisi, D. Riccio, and M. Schwäbisch, "SIR-C/X-SAR multifrequency multipass interferometry: A new tool for geological interpretation," *J. Geophys. Res.*, vol. 101, no. E10, pp. 23 127–23 148, 1995.
[21] R. Lanari, P. Lundgren, M. Manzo, and F. Casu, "Satellite radar interferometry time series analysis of surface deformation for Los Angeles, California," *Geophys. Res. Lett.*, vol. 31, no. 23, p. L23 613, 2004, DOI: 10.1029/2004GL021294.
[22] M. Manzo, G. P. Ricciardi, F. Casu, G. Ventura, G. Zeni, S. Borgström, P. Berardino, C. Del Gaudio, and R. Lanari, "Surface deformation analysis in the Ischia Island (Italy) based on spaceborne radar interferometry," *J. Volcanol. Geotherm. Res.*, vol. 151, no. 4, pp. 399–416, Mar. 2006.
[23] F. Casu, M. Manzo, and R. Lanari, "A quantitative assessment of the SBAS algorithm performance for surface deformation retrieval from DInSAR data," *Remote Sens. Environ.*, vol. 102, no. 3/4, pp. 195–210, Jun. 2006.
[24] P. Tizzani, P. Berardino, F. Casu, P. Euillades, M. Manzo, G. P. Ricciardi, G. Zeni, and R. Lanari, "Surface deformation of Long Valley Caldera and Mono Basin, California investigated with the SBAS-InSAR approach," *Remote Sens. Environ.*, vol. 108, no. 3, pp. 277–289, Jun. 2007.
[25] R. Lanari, F. Casu, M. Manzo, G. Zeni, P. Berardino, M. Manunta, and A. Pepe, "An overview of the small baseline subset algorithm: A DInSAR technique for surface deformation analysis," *Pure Appl. Geophys. (PAGEOPH)*, vol. 164, no. 4, pp. 637–661, Apr. 2007.
[26] R. Lanari, F. Casu, M. Manzo, and P. Lundgren, "Application of SBAS-DInSAR technique to fault creep: A case study of the Hayward Fault, California," *Remote Sens. Environ.*, vol. 109, no. 1, pp. 20–28, Jul. 2007.
[27] M. Neri, F. Casu, V. Acocella, G. Solaro, S. Pepe, P. Berardino, E. Sansosti, T. Caltabiano, P. Lundgren, and R. Lanari, "Deformation and eruptions at Mt. Etna (Italy): A lesson from 15 years of observations," *Geophys. Res. Lett.*, vol. 36, no. 2, p. L02 309, 2009, DOI: 10.1029/2008GL036151.
[28] G. A. Arciniegas, W. Bijker, N. Kerle, and V. A. Tolpekin, "Coherence- and amplitude-based analysis of seismogenic damage in Bam, Iran, using ENVISAT ASAR data," *IEEE Trans. Geosci. Remote Sens.*, vol. 45, pt. 1, no. 6, pp. 1571–1581, Jun. 2006.
[29] T. Scambos, M. Dutkiewicz, J. Wilson, and R. Bindschadler, "Application of image cross-correlation to the measurement of glacier velocity using satellite image data," *Remote Sens. Environ.*, vol. 42, no. 3, pp. 177–186, Dec. 1992.
[30] Y. Fialko and M. Simons, "The complete (3-D) surface displacement field in the epicentral area of the 1999 Mw 7.1 Hector Mine earthquake California from space geodetic observations," *Geophys. Res. Lett.*, vol. 28, no. 16, pp. 3063–3066, Aug. 2001.
[31] T. Strozzi, A. Luckman, T. Murray, U. Wegmüller, and C. L. Werner, "Glacier motion estimation using SAR offset-tracking procedures," *IEEE Trans. Geosci. Remote Sens.*, vol. 40, no. 11, pp. 2384–2391, Nov. 2002.
[32] S.-H. Yun, H. Zebker, P. Segall, A. Hooper, and M. Poland, "Interferogram formation in the presence of complex and large deformation," *Geophys. Res. Lett.*, vol. 34, no. 12, p. L12 305, 2007.
[33] A. Luckman, D. Quincey, and S. Bevan, "The potential of satellite radar interferometry and feature tracking for monitoring flow rates of Himalayan glaciers," *Remote Sens. Environ.*, vol. 111, no. 2/3, pp. 172–181, Nov. 2007.
[34] R. Grandin, A. Socquet, R. Binet, Y. Klinger, E. Jacques, J.-B. de Chabalier, G. C. P. King, C. Lasserre, S. Tait, P. Tapponnier, A. Delorme, and P. Pinzuti, "September 2005 Manda Hararo-Dabbahu rifting event, Afar (Ethiopia): Constraints provided by geodetic data," *J. Geophys. Res.*, vol. 114, no. B8, p. B08 404, Aug. 2009.
[35] A. B. Giles, R. A. Massom, and R. C. Warner, "A method for subpixel scale feature-tracking using Radarsat images applied to the Mertz Glacier Tongue, East Antarctica," *Remote Sens. Environ.*, vol. 113, no. 8, pp. 1691–1699, Aug. 2009.
[36] E. Sansosti, P. Berardino, M. Manunta, F. Serafino, and G. Fornaro, "Geometrical SAR image registration," *IEEE Trans. Geosci. Remote Sens.*, vol. 44, no. 10, pp. 2861–2870, Oct. 2006.
[37] F. Amelung, S. Jonsson, H. Zebker, and P. Segall, "Widespread up-lift and 'trapdoor' faulting on Galápagos volcanoes observed with radar interferometry," *Nature*, vol. 407, no. 6807, pp. 993–996, Oct. 2000.
[38] P. A. Rosen, S. Hensley, G. Peltzer, and M. Simons, "Updated repeat orbit interferometry package released," *EOS*, vol. 85, no. 5, p. 47, Feb. 2004.
[39] R. Michel, J.-P. Avouac, and J. Taboury, "Measuring ground displacements from SAR amplitude images: Application to the Landers earthquake," *Geophys. Res. Lett.*, vol. 26, no. 7, pp. 875–878, Apr. 1999.
[40] E. Pathier, E. J. Fielding, T. J. Wright, R. Walker, B. E. Parsons, and S. Hensley, "Displacement field and slip distribution of the 2005 Kashmir earthquake from SAR imagery," *Geophys. Res. Lett.*, vol. 33, no. 20, p. L20 310, 2006, DOI: 10.1029/2006GL027193.
[41] F. Gatelli, A. Monti Guarnieri, F. Parizzi, P. Pasquali, C. Prati, and F. Rocca, "The wave-number shift in SAR interferometry," *IEEE Trans. Geosci. Remote Sens.*, vol. 32, no. 4, pp. 855–865, Jul. 1994.
[42] F. Rocca, "Modeling interferogram stacks," *IEEE Trans. Geosci. Remote Sens.*, vol. 45, no. 10, pp. 3289–3299, Oct. 2007.
[43] D. Geist, K. Harpp, T. Naumann, M. Poland, W. Chadwick, M. Hall, and E. Rader, "The 2005 eruption of Sierra Negra volcano, Galápagos," *Bull. Volcanol.*, vol. 70, no. 6, pp. 655–673, Apr. 2008.
[44] W. W. Chadwick, D. Geist, S. Jonsson, M. Poland, D. Johnson, and C. Meertens, "Volcano bursting at the seams: Inflation, faulting, and eruption at Sierra Negra volcano, Galápagos," *Geology*, vol. 34, no. 12, pp. 1025–1028, Dec. 2006.
[45] N. B. D. Bechor and H. A. Zebker, "Measuring two-dimensional movements using a single InSAR pair," *Geophys. Res. Lett.*, vol. 33, no. 16, p. L16 311, Aug. 2006, DOI: 10.1029/2006GL026883.

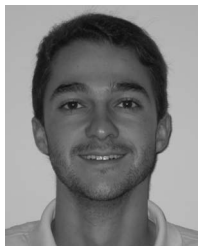

Francesco Casu received the Laurea degree (*summa cum laude*) and the Ph.D. degree in electronic engineering from the University of Cagliari, Cagliari, Italy, in 2003 and 2009, respectively.

Since 2003, he has been with the Istituto per il Rilevamento Elettromagnetico dell'Ambiente (IREA), Italian National Research Council (CNR), Napoli, Italy, where he currently holds a permanent Researcher position. He was a Visiting Scientist with the University of Texas at Austin, Austin, in 2004, the Jet Propulsion Laboratory, Pasadena, CA, in 2005, and the Department of Geophysics, Stanford University, Stanford, CA, in 2009. His main research interests are in the DInSAR field, in the multipass interferometry (particularly concerning the improvement of the SBAS-DInSAR algorithm), and in the SBAS-DInSAR measurement assessment. He is currently involved in the development and application of DInSAR techniques to data acquired by novel generation satellites such as COSMO-SkyMed, TerraSAR-X and ALOS-PALSAR.

Andrea Manconi was born in 1978. He received the M.S. degree in environmental engineering from the University of Cagliari, Cagliari, Italy, in 2005 and the Ph.D. degree (*magna cum laude*) in geophysics from the University of Potsdam, Potsdam, Germany, in 2009.

After his graduation, he has been Visiting Researcher at the GeoForschungsZentrum Potsdam. In February 2009, he was with the Istituto per il Rilevamento Elettromagnetico dell'Ambiente (IREA), Italian National Research Council (CNR), Naples, Italy. Since November 2010, he has been with the IRPI-CNR, Turin, Italy. His research interests mainly concern the analysis and modeling of surface displacements measured via differential SAR interferometry in volcanic and seismogenetic areas.

Antonio Pepe was born in 1974. He received the Laurea degree in electronic engineering and the Ph.D. degree from the University of Napoli Federico II, Naples, Italy, in 2000 and 2007, respectively.

After graduation, he was with the Istituto per il Rilevamento Elettromagnetico dell'Ambiente (IREA), Italian National Research Council (CNR), Naples, Italy, where he currently occupies the position of Researcher. He was a Visiting Scientist at University of Texas at Austin, Austin, in 2005, and at the Jet Propulsion Laboratory (JPL), Caltech, Pasadena, CA, in 2009. His main research interests concern the differential SAR interferometry applications for the monitoring of surface displacements, such as those produced by subsidence, volcano activity, and earthquakes.

Riccardo Lanari (M'91–SM'01) was born in Napoli, Italy, in 1964. He received the Laurea degree (*summa cum laude*) in electronic engineering from the University of Napoli Federico II, Naples, Italy, in 1989.

In the same year, following a short experience at ITALTEL SISTEMI SPA, he was with IRECE and after Istituto per il Rilevamento Elettromagnetico dell'Ambiente (IREA), a Research Institute of CNR (the Italian National Council of Research), where he currently occupies the position of Senior Researcher. He has been a Visiting Scientist at different foreign research institutes, including the Institute of Space and Astronautical Science (ISAS), Japan (1993), the German Aerospace Research Establishment (DLR), Germany (1991 and 1994), and the Jet Propulsion Laboratory (JPL), Pasadena, CA, in 1997, 2004, and 2008, where he received a NASA recognition for the technical developments related to the SRTM mission. He has lectured in several national and foreign universities and research centers; he has been adjunct professor of Electrical Communication at the l'Università del Sannio (Benevento) from 2000 to 2003 and, from 2000 to 2008, Lecturer of the SAR module course of the International Master in Airbone Photogrammetry and Remote Sensing, offered by the Institute of Geomatics in Barcelona (Spain). He is the holder of two patents, has authored or coauthored more than 60 international journal papers and, in 1999, the book entitled *Synthetic Aperture Radar Processing* (CRC-Press). His main research activities are in the synthetic aperture radar (SAR) data processing field as well as in SAR interferometry techniques.

Dr. Lanari is a Distinguished Speaker of the Geoscience and Remote Sensing Society of IEEE, and he has served as Chairman and technical program committee member at several international conferences. Moreover, he acts as Reviewer of several peer-reviewed international journals.